ACS APPLIED MATERIALS & INTERFACES

Research Article

www.acsami.org

Microwave Heating of Functionalized Graphene Nanoribbons in Thermoset Polymers for Wellbore Reinforcement

Nam Dong Kim,[†,#] Andrew Metzger,[†,#] Vahid Hejazi,[‡] Yilun Li,[†] Anton Kovalchuk,[†] Seoung-Ki Lee,[†] Ruquan Ye,[†] Jason A. Mann,[†] Carter Kittrell,[†] Rouzbeh Shahsavari,*[,‡,§,∥] and James M. Tour*[,†,§,∥]

[†]Department of Chemistry, [‡]Department of Civil and Environmental Engineering, [§]The NanoCarbon Center, and [∥]Department of Material Science and NanoEngineering, Rice University, 6100 Main Street, Houston, Texas 77005, United States

Supporting Information

ABSTRACT: Here, we introduce a systematic strategy to prepare composite materials for wellbore reinforcement using graphene nanoribbons (GNRs) in a thermoset polymer irradiated by microwaves. We show that microwave absorption by GNRs functionalized with poly(propylene oxide) (PPO-GNRs) cured the composite by reaching 200 °C under 30 W of microwave power. Nanoscale PPO-GNRs diffuse deep inside porous sandstone and dramatically enhance the mechanics of the entire structure via effective reinforcement. The bulk and the local mechanical properties measured by compression and nanoindentation mechanical tests, respectively, reveal that microwave heating of PPO-GNRs and direct polymeric curing are major reasons for this significant reinforcement effect.

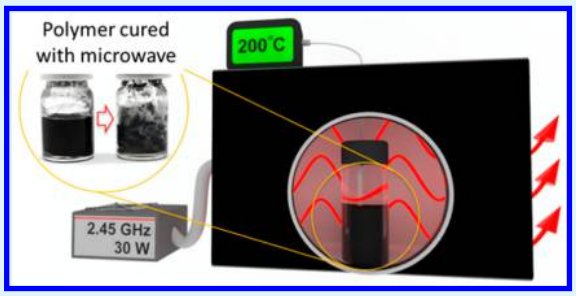

KEYWORDS: *graphene nanoribbon, microwave, microwave induced heating, polymer composite, mechanical reinforcement,*

INTRODUCTION

Wellbore reinforcement in oil and gas recovery has received considerable attention over the last two decades since wellbore instability can lead to substantially higher drilling costs.[1,2] Microfractures present in the rock formation are a common cause of severe wellbore instability because drilling fluid seeps into these fractures thereby inhibiting the stabilizing effect of the drilling fluid overbalance and also reducing borehole pressure integrity by forcing fractures even further apart.[3−5] Therefore, there has been a great deal of effort to stabilize wellbores and prevent fluid loss by using additives, such as mica, calcium carbonate, gilsonite, and asphalt to seal microfractures.[6] However, these attempts have not been widely implemented since the size of conventional additives do not match that of the porous formation and they are far too slow in sealing microfractures. It is therefore recommended that deformable additives be developed with a broad size distribution capable of quickly sealing a wide-range of microfracture openings at an effective concentration that does not adversely affect the functional properties of the drilling fluid.[6]

Carbon nanomaterials have been used as additives for mechanical reinforcement of polymers and have recently shown that they penetrate through porous media.[7,8] Specifically, carbon nanotubes (CNTs) have been explored as polymeric reinforcements because of their small size, high Young's modulus, high tensile strength, and low percolation threshold.[9−16] Another remarkable property of CNTs is that they are highly efficient microwave absorbers.[17−21] Although the precise mechanism of CNT microwave interaction is poorly understood, nanotubes generate intense heat that could be used in a thermoset polymer for rapid curing at much lower microwave powers than those currently used in microwave assisted polymer curing (~900 W).[22−24] However, concerns over their toxicity as well as problems in preparing homogeneous CNT dispersions have plagued their commercial deployment.[25,26] Alternatively, graphene nanoribbons (GNRs), which are ribbon-like graphene made from chemically unzipping CNTs,[27] are now being considered for use as polymer reinforcements because of their remarkably low percolation threshold, high load transfer capability, and low toxicity.[28−30]

This Research Article shows a proof of concept for wellbore strengthening by microwave heating functionalized GNRs dispersed in an oil-based thermoset polymer to rapidly cross-link the matrix and thereby increase its mechanical resilience within sandstone. Poly(propylene oxide) (PPO) functionalization of the GNRs not only increased their dispersibility in the oil-based drilling fluid but also increased the amount of heat released by the GNRs under microwave irradiation, likely due to their superior dispersion. The temperature of the PPO-GNR polymer suspension dramatically increased above 200 °C within minutes under very low microwave power (30 W). The intense, localized heat from the PPO-GNRs cured the polymer within a short period of time producing both enhanced reinforcement and mechanical integrity of sandstone because of the improved

Received: February 10, 2016
Accepted: May 3, 2016
Published: May 3, 2016

DOI: 10.1021/acsami.6b01756
ACS Appl. Mater. Interfaces 2016, 8, 12985−12991

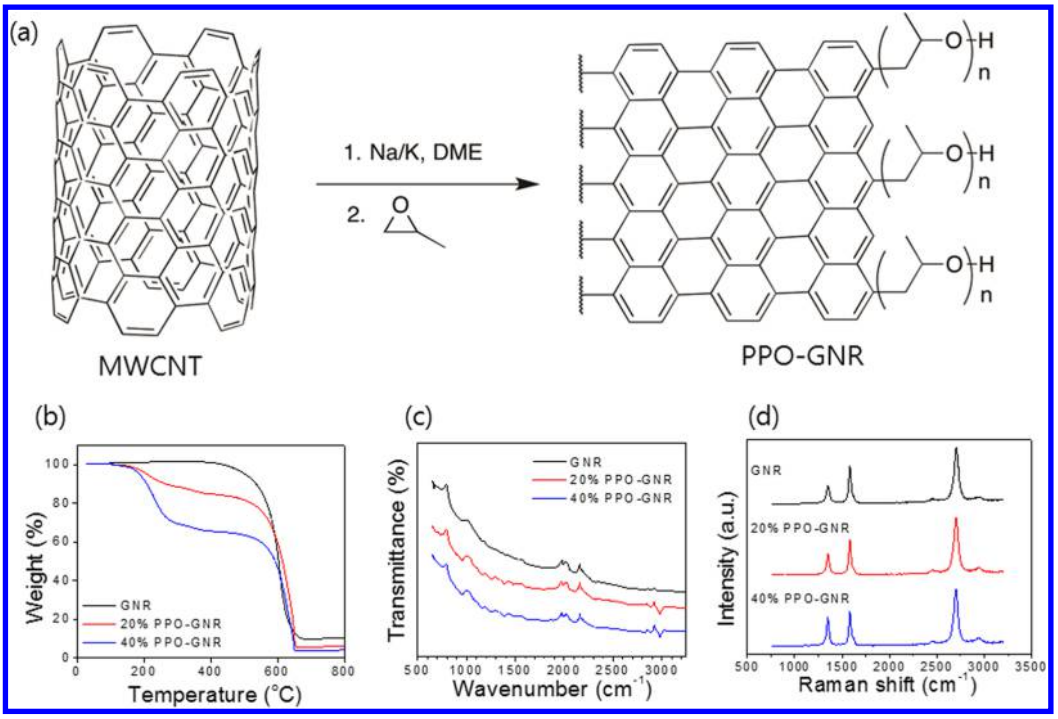

Figure 1. (a) Synthesis of PPO-GNRs from MWCNTs. Only one tube within the MWCNT is represented. Characterization of GNRs and PPO-GNRs by (b) TGA, (c) FT-IR, and (d) Raman.

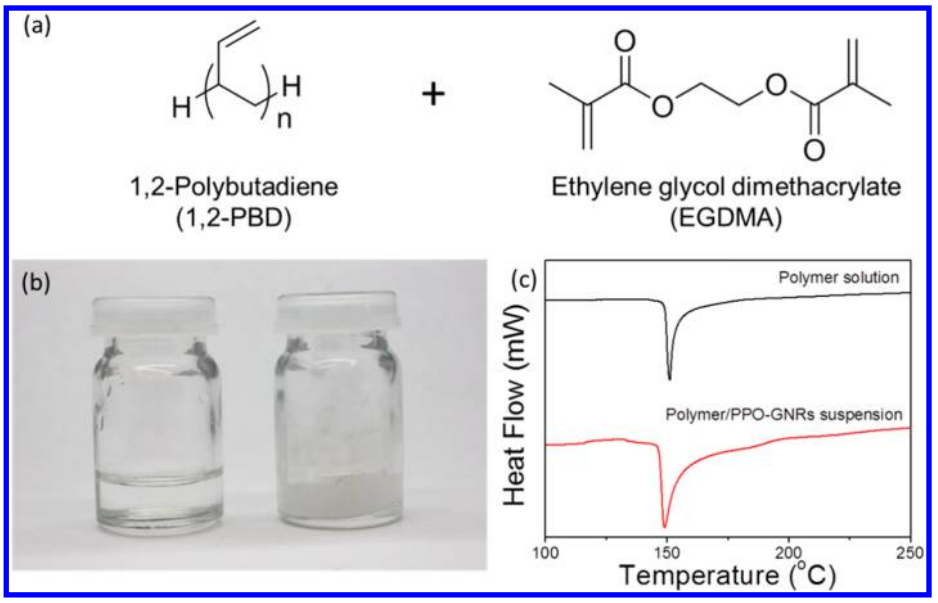

Figure 2. (a) Chemical structures of the polymer and cross-linker. (b) Image of the thermoset polymer stock solution before and after curing in an oven at 200 °C. (c) DSC characterization of the polymer solution and polymer/PPO-GNRs suspension.

load transfer characteristics from the microwave curing process. This method not only provides a simple and cost-effective way to prepare polymer/carbon nanomaterial reinforced composites, but also may be useful in extreme downhole conditions provided that there is a microwave source tool following the drill head.

RESULTS AND DISCUSSION

Our first goal was to synthesize GNRs that were soluble in an organic phase and aqueous phase, since both types of drilling fluids are used in industry. As prepared, GNRs have protons at the edges and showed poor dispersibility (Figure S1) in both water and Escaid110 (a commercially available mineral oil based drilling fluid).[28] However, GNRs functionalized with PPO emanating from their edges showed good dispersion in both water and Escaid 110 (Figure 1a and Figure S1). Thermogravimetric analysis (TGA) showed gradual weight loss between 200 and 400 °C because of the decomposition of PPO (Figure 1b) thus confirming that 20% (20%-PPO-GNR) and 40% (40%-PPO-GNR) of PPO was functionalized on the GNR surface depending on the synthesis method. The presence of PPO was confirmed by Fourier transform infrared (FT-IR) analysis (Figure 1c) with a characteristic peak at 2950 cm^{-1} indicative of C−H stretches. Raman spectroscopy (Figure 1d)

DOI: 10.1021/acsami.6b01756
ACS Appl. Mater. Interfaces 2016, 8, 12985−12991

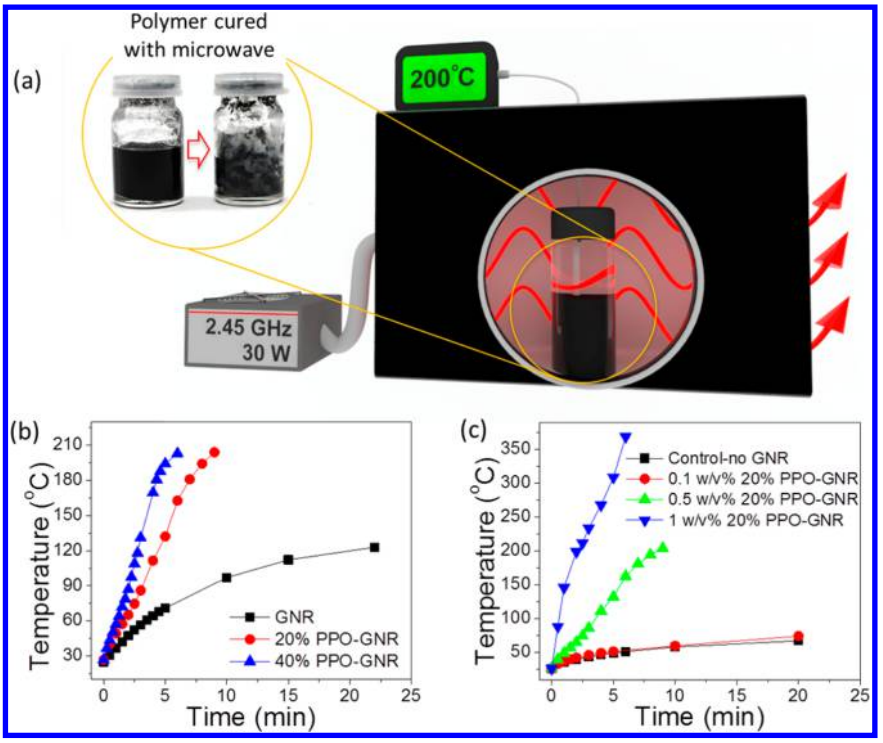

Figure 3. Microwave-assisted curing of polymer/PPO-GNR suspensions. (a) Illustration of the microwave-assisted polymer curing system using a waveguide and an in situ temperature monitor with a photograph of the polymer/PPO-GNRs suspension before and after microwave curing. (b) Microwave heating profile of GNR, 20%-PPO-GNR, and 40%-PPO-GNR suspensions. (c) Microwave heating profile of the polymer/PPO-GNR suspension containing different amounts of 20%-PPO-GNR.

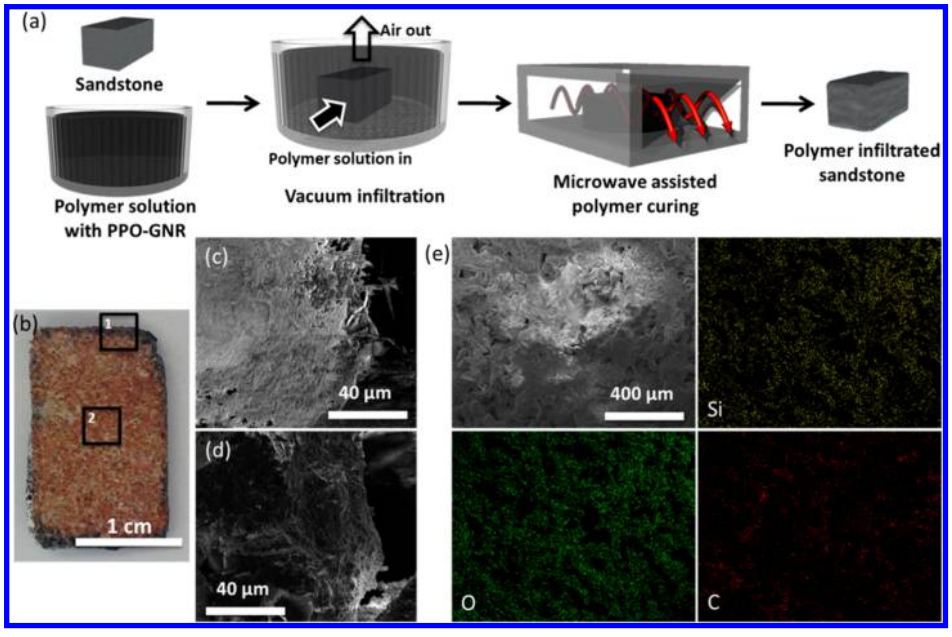

Figure 4. (a) Experimental scheme for preparation of microwave-cured polymer/PPO-GNR infiltrated sandstone (SPG-M). (b) Photograph of the cross-section of SPG-M. The black squares, 1 and 2, correspond to SEM images c and d, respectively. (e) SEM image of the inside of SPG-M and corresponding EDX elemental mapping of Si, O, and C.

showed that the D/G ratios (0.48, 0.61, 0.84 for GNR, 20%-PPO-GNR, and 40%-PPO-GNR, respectively) increased with the amount of PPO functionalization due to the increased C-sp^3 content.

Before making a polymeric composite with PPO-GNRs, a suitable thermoset polymer should be selected that is readily available for curing at moderate temperatures. In addition, there are several criteria that must be considered in order to be an adequate thermoset polymer for downhole applications. First, polymerization needs to be done very quickly before fluid loss occurs thus reactive species are required. Second, the polymer should have a relatively high curing temperature to ensure that the high inherent temperature conditions (~70 °C) in the

DOI: 10.1021/acsami.6b01756
ACS Appl. Mater. Interfaces 2016, 8, 12985−12991

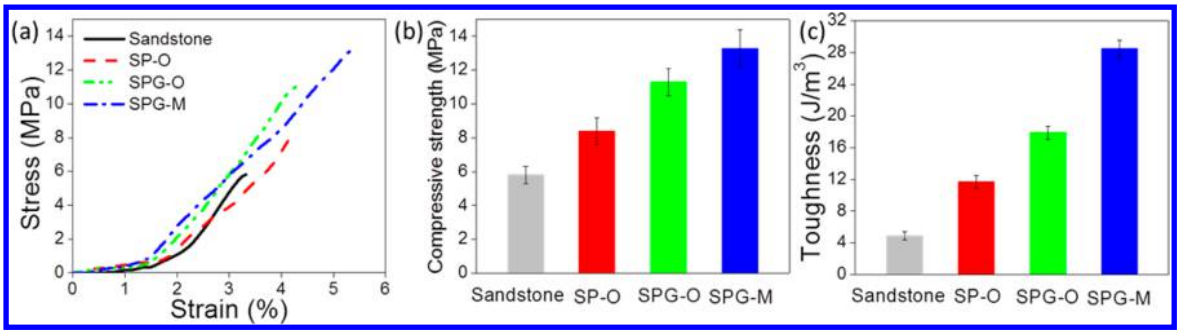

Figure 5. Compression mechanical tests of sandstone alone and polymer/PPO-GNRs infiltrated sandstones cured either by convective oven or microwaves. (a) Stress versus strain plot, (b) maximum compressive strength, and (c) toughness. Note: SP = sandstone infiltrated with polymer alone, SPG = sandstone infiltrated with polymer/PPO-GNRs, O = oven cured, and M = microwave cured.

wellbore do not prematurely result in cross-linking. Third, it must be inexpensive. And finally of low toxicity.

Given these selection criteria, we chose 1,2-polybutadiene (1,2-PBD) and ethylene glycol dimethacrylate (EGDMA) as the polymer backbone and cross-linking monomer, respectively (Figure 2a and Figure S2). A cross-linking polymer stock solution (Figure 2b) was prepared by mixing 1,2-PBD/EGDMA into Escaid110, which could then be heat cured in a 200 °C oven producing a rigid white polymer block. Differential scanning calorimetry (DSC) showed a sharp exothermic characteristic at 150 °C arising from its phase transition during curing (Figure 2c).

Figure 3a illustrates the microwave waveguide and in situ temperature monitoring system used in our microwave assisted polymer curing experiments. We tested the microwave heating profile of several carbon materials (Figure S3) and selected GNRs based on their ability to heat and their low toxicity. Figure 3b shows the heating profile of GNRs alone and PPO-GNRs with increasing amounts of PPO, but a fixed amount of GNRs (0.5 w/v%) in the polymer stock solution. The polymer/GNR suspension slowly heats under microwave exposure and did not increase in temperature to >120 °C. However, PPO-GNRs show a much faster heating rate with an increase in temperature up to 200 °C within 10 min. 40%-PPO-GNR showed higher heating rates than 20%-PPO-GNR presumably due to the higher dispersibility in the oil-based polymer solution. However, extremely rapid heating and very high temperatures of the polymer may not be good for curing because it may decompose the polymer or induce excessive outgassing from the composite making it a porous structure. Therefore, further experiments were conducted using different amounts of 20%-PPO-GNR to optimize the process. The polymer stock solution itself did not display any significant microwave heating nor did the addition of a small amount of PPO-GNR (0.1 w/v%) significantly affect its heating rate (Figure 3c). But since 1 w/v% of PPO-GNR heated rapidly to very high temperatures that could damage the polymer backbone, 0.5 w/v% of the 20%-PPO-GNR stock solution was selected for further mechanical testing.

Figure 4a schematically illustrates the process we used to infiltrate a block of porous sandstone with polymer/PPO-GNRs for microwave curing (SPG-M is designated for sandstone polymer-GNR microwave). Vacuum infiltration was used to drive the polymer/PPO-GNRs into the porous sandstone as a mimic for the pressured infiltration of a wellbore environment. A center cut section of the SPG-M showed numerous white spots that are not naturally present (Figure 4b). Scanning electron microscopy (SEM) of SPG-M shows that the polymer and PPO-GNRs form thick film-like structures on the sandstone surface (Figure 4c). In the cross-section of the SPG-M, we observed PPO-GNR strands attached onto the sandstone wall which confirms successful infiltration of the stock polymer/PPO-GNR solution (Figure 4d). As shown in Table S1, energy dispersive X-ray analysis (EDX) of the sandstone before and after addition of polymer/PPO-GNRs revealed that the carbon/oxygen ratio inside the sandstone increased from 0.21 to 0.72 due to infiltration of polymer/PPO-GNRs into the porous sandstone. EDX mapping of the sandstone shows the polymer and carbon nanomaterials were throughout the sandstone (Figure 4e) as further confirmation that the sandstone and polymer composite structure had been successfully prepared.

Figure 5 shows the ensemble mechanical properties from the compression experiments on the polymer-infiltrated sandstone. The compression system using the parallel bottom and top platens to apply uniaxial force develops a rather complex system of stresses due to the end restraints by the platens. However, because of Poisson's effect, the samples all undergo lateral expansion which results in creating cracks and eventually leads to failure of the samples (Figure S4). To compare the properties of SPG-M, several control samples were prepared using a convective oven to cure the materials. These control sandstone samples SP-O and SPG-O were cured in an oven without and with PPO-GNRs, respectively (O refers to oven-cured). By comparing these materials, the effect of either the addition of PPO-GNRs or microwave assisted polymer curing on the mechanical performance reinforcement was investigated.

Addition of polymer alone inside the sandstone increased the maximum compressive strength of the sandstone from 5.8 to 8.4 MPa (Figure 5a,b). This agrees well with the common intuition about such rock-type materials wherein the lower the porosity, the higher the compressive strength. However, with addition of PPO-GNRs, the maximum compressive strength of the SPG-M sample increased even higher to 11.3 MPa. Assuming equivalent porosities for oven cured sandstones infiltrated by polymer alone (SP-O) or polymer/PPO-GNRs (SPG-O), the ~35% increase in the compressive strength of SPG-O compared to SP-O is likely due to 1) the reinforcing effect of GNRs, which strengthen its surrounding matrix,[28] and 2) the high thermal conductivity of the GNRs, which causes more adequate and rapid curing of the polymer in SPG-O compared to SP-O, resulting in a more efficient high-strength adhesive bonding between polymer and sandstone. More impressive enhancement in reinforcement can be found in SPG-M, where the maximum compressive strength of SPG-M (13.3 MPa) increased more than 130% compared to that of

DOI: 10.1021/acsami.6b01756
ACS Appl. Mater. Interfaces 2016, 8, 12985−12991

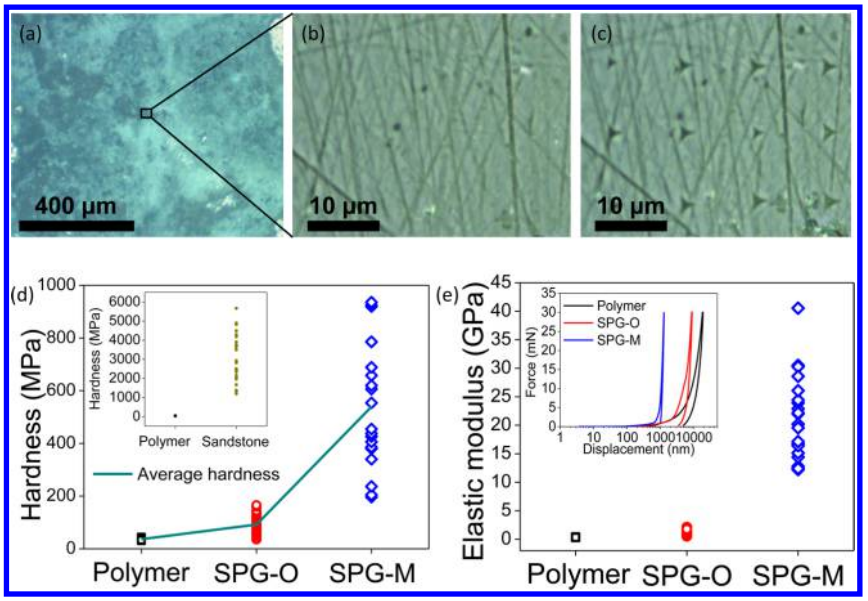

Figure 6. Nanoindentation test for the effect of microwave-assisted cured polymer on mechanical enhancement. (a) Optical image of the SPG-M sample before indentation experiments. Enlarged images (b) before and (c) after indentation. A part of the 10 × 10 matrix of indentation imprints (triangles) can be seen in panel c. (d) Hardness values from nanoindentation experiments for polymer alone, SPG-O, and SPG-M. Inset shows difference of hardness between polymer and sandstone. (e) Elastic modulus value from the nanoindentation experiments for polymer, SPG-O, and SPG-M.

pure sandstone, and is even ∼18% higher than that of SPG-O, the oven cured equivalent.

Such a strong reinforcement in SPG-M can be understood by comparing microwave assisted heating to convective heating of the polymer in SPG-O. In the oven-heated thermoset polymer, GNRs are just one part of a physical mixture inside the composite. Due to the low thermal diffusion through the sandstone and also through the nonuniformly distributed pores filled by polymer, heat cannot be homogeneously transferred to the GNRs dispersed in the polymer. However, with microwaves, each GNR absorbs microwave energy independently and acts as a nanoscale heat generator with local temperatures that are high enough to thoroughly cure the surrounding polymer. Moreover, since the GNRs generate heat to induce polymerization, it can be assumed that the interface between the GNR and polymer has greater van der Waals interactions and will provide a more effective load transfer for stronger reinforcement than SPG-O. It could also be that the polymer chains added into the planes of the GNRs, but that was not confirmed here.

Furthermore, we know that GNRs toughen related polymers.[28,31] Here, the total toughness of the SPG-M (28.5 GPa) was ∼1.6× higher than that of SPG-O, and also ∼6× greater than that of pure sandstone (4.9 GPa) (Figure 5c). Toughness is defined as the amount of energy a material absorbs before failure (representing the work-of-fracture), which is different from the classical "fracture toughness" with the unit of $P_a\sqrt{m}$. The work-of-fracture is the area under the stress−strain curve, which is deeply affected by gradual, "graceful fracture", whereas the fracture toughness does not incorporate this entire process.[9]

To investigate the micromechanics of the samples and to study the microstructural reinforcement effects of GNRs, a matrix-based algorithm was developed to conduct hundreds of indentations on the surface of the samples to directly obtain the mechanics of individual phases of the samples. The nanoindentation measurements were conducted by indenting 100 spots in a 10 × 10 matrix form using a Berkovich tip with a size of ∼50 nm, which allowed us to investigate the mechanical properties of the composite structure on both the nanometer and micrometer scales. Figure 6a and b shows the surface of the SPG-M sample before indentation. Some imprints (triangles) of the indentation on the sample surface can be seen in Figure 6c after unloading.

From the control experiments for the polymer and sandstone, the hardness value (which relates to strength) was found to be 30 MPa for the polymer alone, and over 1000 MPa for the sandstone alone (Figure 6d inset). Therefore, to compare the mechanical reinforcement contribution of the polymer, hardness values larger than 1000 MPa were excluded from further analysis as they would correspond to the sandstone alone and not the cured polymer/PPO-GNRs. As GNRs were introduced to the polymer in the SPG-O, the hardness of the polymer was increased up to 180 MPa. However, for SPG-M, hardness values were >200 MPa with values ranging from 200 to 900 MPa (Figure 6d). The variation is due to the localized grid-like indented spots, which may or may not be in the vicinity of the GNRs. Nevertheless, the average hardness (∼600 MPa) of all these spots in SPG-M is significantly higher than the average hardness of SPG-O (∼100 MPa). Considering the measurement capabilities of nanoindentation (50 nm tip size and ∼10 μm distance between the indentation spots), our results show the enhanced mechanical properties of SPG-M are mainly due to the strong interaction between GNRs and the polymer, which improves the cross-linking and mechanical integrity of the polymer upon microwave irradiation. The elastic modulus of the samples was also calculated using the load−displacement curves (inset of Figure 6e). All $P-h$ curves in this figure showed smooth shapes and no pop-in behavior could be detected. The lower displacement of the SPG-M at the peak force indicates the higher hardness of this sample, compared to SPG-O/SP-O, resulting in lower material deformation. SPG-M also showed a highly enhanced elastic modulus compared to SPG-O owing to

DOI: 10.1021/acsami.6b01756
ACS Appl. Mater. Interfaces 2016, 8, 12985−12991

the incorporation of stiff GNR fillers into the polymer chains resulting in a stiffer composite material (Figure 6e). These results indeed demonstrate that microwave assisted polymer curing in the presence of carbon nanomaterials can be a highly efficient for structural reinforcement.

CONCLUSION

In summary, we demonstrated that the use of GNRs as highly efficient fillers in polymers, combined with microwave-assisted localized heating, results in the significantly improved mechanical properties of polymer reinforced sandstone. Systematic investigation of the mechanical properties (e.g., strength, toughness, and stiffness) of the polymer-reinforced sandstone at multiple length scales suggests that the interaction of carbon nanomaterials with a polymer matrix provides enhanced reinforcement even with a very low amount of carbon filler. Finally, while we showcased the benefits of this approach in the context of enhancing the mechanics of porous sandstones and wellbore reinforcements, the concepts and strategies of this work, especially the use of low power microwave energy, can be easily applicable to a variety of porous materials and extreme conditions such as those found underground or in outer space. Although this study focused on using GNRs, alternative graphitic materials that are microwave responsive can be explored.

EXPERIMENTAL SECTION

Synthesis of PPO-GNRs. GNRs were prepared by Na/K-induced longitudinal splitting of multiwalled carbon nanotubes (MWCNTs).[32] We adapted this method for the synthesis of polypropylene-oxide functionalized GNRs (PPO-GNRs). First, MWCNTs (500 mg) were placed in a dried and septum-sealed flask, purged with nitrogen followed by the addition of 250 mL of freshly distilled dimethyl ether, and the mixture was bath sonicated for 30 min. Na/K alloy (0.80 mL) was carefully injected into the reaction flask via syringe and the mixture stirred at room temperature for 72 h. Propylene oxide (1 mL) was then injected into the reaction flask, the mixture was stirred at room temperature for 24 h, and then quenched by addition of methanol (5 mL). The resulting PPO-GNRs were isolated via vacuum filtration over a 0.45 μm PTFE filter and washed sequentially with deionized water, methanol, acetone, and diethyl ether. The product was dried under vacuum at 60 °C for 24 h to produce ∼750 mg of 20%-PPO containing GNRs (20%-PPO-GNR). For the synthesis of 40%-PPO-GNR, we doubled the amount of propylene oxide (2 mL), while the amount of other reagents remained the same, which produced ∼1000 mg of 40%-PPO-GNR. Synthesized materials were characterized by thermogravimetric analysis (Q50, TA Instruments), FT-IR spectroscopy (Nicolet Nexus 870, Thermo Fisher Scientific), and Raman spectroscopy (inVia micro Raman, Renishaw).

Preparation of Polymer/PPO-GNR Stock Solution. 1,2-PBD (Sigma-Aldrich, CAS no. 9003-17-2) was selected as a polymer backbone and EGDMA (Sigma-Aldrich, CAS no. 97-90-5) as a cross-linking agent. A polymer stock solution was prepared by first mixing 2 g of 1,2-PBD with 64 mL of EGDMA (which corresponds to a 1:10 molar ratio of butadiene repeating groups and EGDMA), then mixing the polymer solution with Escaid110 in a 1:1 volume ratio. This ratio of very high cross-linking component was selected because of the high rate of cross-linking that will be needed in the downhole drilling environment. To prepare a polymer/PPO-GNR suspension, PPO-GNRs were added to the polymer stock solution (1,2-PBD/EGDMA/Escaid110) in different w/v% (note, 10 mg/mL = 1 w/v%). As a control, we also prepared a polymer/GNR suspension using the same polymer stock solution mixed with GNRs alone.

Microwave Heating and Curing of Polymer/PPO-GNRs. Our experimental system consisted of a variable power (10−70 W) 2.45 GHz microwave generator, a thermocouple (stainless steel shielded, ungrounded K-type, d = 0.5 mm) for in situ temperature monitoring, and waveguide which directs the microwaves onto the sample (Figure S5). The waveguide provides well-defined field intensity within its central region to uniformly irradiate the sample. The polymer/PPO-GNRs suspension was placed inside a waveguide under 30 W of microwave irradiation and after the temperature reached ∼200 °C, the entire suspension was cured and formed a dark gray composite. Any possible microwave absorbing properties of the thermocouple was taken into account by measuring the temperature increase recorded (40−50 °C) when the thermocouple alone was exposed to microwave radiation.

Microwave Heating and Curing of Polymer/PPO-GNRs Solution in Sandstone. A porous sandstone block (19 mm × 19 mm × 12.7 mm; Dundee, Cleveland Quarries, ∼9 g) was immersed into a polymer/PPO-GNR suspension in a 20 mL glass container and placed under vacuum (−100 kPa) to drive the suspension into the sandstone. The polymer/PPO-GNR suspension-infiltrated sandstone was then placed within the middle of the waveguide and exposed to 30 W of microwave irradiation. The SPG-M sample reached a temperature of 200 °C within ∼3 min and was held at that temperature for another 10 min with the continued irradiation. The microwave source was then turned off, the sandstone composite was permitted to cool. As a control, we also prepared SP-O and SPG-O which were cured in an oven without and with PPO-GNRs, respectively.

Mechanical Strength Testing of Polymer/PPO-GNRs Infiltrated Sandstone. A conventional static compression test was carried out on the SPG-M using an Instron Dual Column Universal Testing System (Model 4500) with a 100 kN load cell to measure the bulk mechanical properties. Uniaxial compression loading was applied until the failure cracks, approximately parallel to the direction of the applied load, appeared on the side of the samples and then the sample crushed. An Anton-Paar nanoindentation tester (NHT^2) equipped with the diamond Berkovich tip was used to collect local surface mechanical characterization data by indenting to depths at the nano- and micrometer scales. A grid technique was used for the indentation tests (100 points in the shape of a 10 × 10 matrix where each point is 10 μm apart). Before testing, the surface of the samples was ground with sandpaper (hand ground using sandpaper grade from 200 to 2000) and cleaned with a soft cloth to provide a smooth surface relevant for indentation testing. The nanoindentation was set to the force-controlled mode to apply a maximum force of 30 mN in each indent. A trapezoidal loading−unloading cycle was used which consists of the 3 stages, that is, loading to maximum force, holding for 5 s at the peak load, and unloading periods (Figure S6) Next, from the load−displacement of nanoindentation, $P-h$ curves, we obtained the elastic modulus (E), and hardness (H) using eqs 1 and 2

$$E = \frac{\frac{0.5\pi S}{\sqrt{a}}}{1 - \nu^2} \quad (1)$$

$$H = \frac{P_{max}}{a} \quad (2)$$

where a is the contact area at P_{max}, S is the slope of the unloading curve, and ν is Poisson's ratio.[33]

ASSOCIATED CONTENT

Supporting Information

The Supporting Information is available free of charge on the ACS Publications website at DOI: 10.1021/acsami.6b01756.

Dispersibility of GNRs and PPO-GNRs both in water and Escaid 110, microwave heating of several carbon nanomaterials, thermal curing test of 1,2-PBD with different methacrylates, EDX analysis of sandstone, SPG-M sample images before and after compression mechanical testing, schematic illustration of microwave curing system, and representative trapezoidal loading and force versus time plot of nanoindentation (PDF)

DOI: 10.1021/acsami.6b01756
ACS Appl. Mater. Interfaces 2016, 8, 12985−12991

AUTHOR INFORMATION

Corresponding Authors

*E-mail: rouzbeh@rice.edu

*E-mail: tour@rice.edu.

Author Contributions

#These authors contributed equally.

Notes

The authors declare no competing financial interest.

ACKNOWLEDGMENTS

This work was partially supported by MI-SWACO, a Schlumberger company.

REFERENCES

(1) McLean, M. R.; Addis, M. A. Wellbore Stability: The Effect of Strength Criteria on Mud Weight Recommendations. Presented at the 65th Annual Technical Conference and Exhibition, New Orleans, 23–26 October 1990, DOI: 10.2118/20405-MS.

(2) Morita, N.; Fuh, G.-F. Parametric Analysis of Wellbore-Strengthening Methods From Basic Rock Mechanics. *SPE Drill. Completion* **2012**, *27*, 315–327.

(3) Wang, H.; Towler, B. F.; Soliman, M. Y. Fractured Wellbore Stress Analysis: Sealing Cracks To Strengthen a Wellbore. Presented at SPE/IADC Drilling Conference, Amsterdam, The Netherlands, 20–22 February 2007, DOI: 10.2118/104947-MS.

(4) Chen, X.; Tan, C. P.; Detournay, C. The Impact of Mud Infiltration on Wellbore Stability in Fractured Rock Masses. Presented at SPE/ISRM Rock Mechanics Conference, Irving, Texas, 20–23 October 2002. DOI: 10.2118/78241-MS.

(5) Sweatman, R.; Kelley, S.; Heathman, J. Formation Pressure Integrity Treatments Optimize Drilling and Completion of HTHP Production Hole Sections. Presented at SPE European Formation Damage Conference, The Hague, The Netherlands, 21–22 May 2001, DOI: 10.2118/68946-MS.

(6) Labenski, F.; Reid, P.; Santos, H. Drilling Fluids Approaches for Control of Wellbore Instability in Fractured Formations. Presented at SPE/IADC Middle East Drilling Technology Conference and Exhibition, Abu Dhabi, United Arab Emirates, 20–22 October 2003, DOI: 10.2118/85304-MS.

(7) Berlin, J. M.; Yu, J.; Lu, W.; Walsh, E. E.; Zhang, L.; Zhang, P.; Chen, W.; Kan, A. T.; Wong, M. S.; Tomson, M. B.; Tour, J. M. Engineered Nanoparticles for Hydrocarbon Detection in Oil-Field Rocks. *Energy Environ. Sci.* **2011**, *4*, 505–509.

(8) Hwang, C.-C.; Wang, L.; Lu, W.; Ruan, G.; Kini, G. C.; Xiang, C.; Samuel, E. L.; Shi, W.; Kan, A. T.; Wong, M. S.; Tomson, M. B.; Tour, J. M. Highly Stable Carbon Nanoparticles Designed for Downhole Hydrocarbon Detection. *Energy Environ. Sci.* **2012**, *5*, 8304–8309.

(9) Sakhavand, N.; Shahsavari, R. Universal Composition–Structure–Property Maps for Natural and Biomimetic Platelet–Matrix Composites and Stacked Heterostructures. *Nat. Commun.* **2015**, *6*, 6523.

(10) Koerner, H.; Price, G.; Pearce, N. A.; Alexander, M.; Vaia, R. A. Remotely Actuated Polymer Nanocomposites——Stress-Recovery of Carbon-Nanotube-Filled Thermoplastic Elastomers. *Nat. Mater.* **2004**, *3*, 115–120.

(11) Stankovich, S.; Dikin, D. A.; Dommett, G. H. B.; Kohlhaas, K. M.; Zimney, E. J.; Stach, E. A.; Piner, R. D.; Nguyen, S. T.; Ruoff, R. S. Graphene-Based Composite Materials. *Nature* **2006**, *442*, 282–286.

(12) Coleman, J. N.; Khan, U.; Blau, W. J.; Gun'ko, Y. K. Small but Strong: A Review of the Mechanical Properties of Carbon Nanotube–Polymer Composites. *Carbon* **2006**, *44*, 1624–1652.

(13) Lau, K.; Gu, C.; Hui, D. A Critical Review on Nanotube and Nanotube/Nanoclay Related Polymer Composite Materials. *Composites, Part B* **2006**, *37*, 425–436.

(14) Li, Y.; Wang, K.; Wei, J.; Gu, Z.; Wang, Z.; Luo, J.; Wu, D. Tensile Properties of Long Aligned Double-Walled Carbon Nanotube Strands. *Carbon* **2005**, *43*, 31–35.

(15) Yu, M.-F.; Lourie, O.; Dyer, M. J.; Moloni, K.; Kelly, T. F.; Ruoff, R. S. Strength and Breaking Mechanism of Multiwalled Carbon Nanotubes Under Tensile Load. *Science* **2000**, *287*, 637–640.

(16) Chen, Y.; Tao, J.; Li, S.; Khashab, N. M. Compositing Polyetherimide with Polyfluorene Wrapped Carbon Nanotubes for Enhanced Interfacial Interaction and Conductivity. *ACS Appl. Mater. Interfaces* **2014**, *6*, 9013–9022.

(17) Imholt, T. J.; Dyke, C. A.; Hasslacher, B.; Perez, J. M.; Price, D. W.; Roberts, J. A.; Scott, J. B.; Wadhawan, A.; Ye, Z.; Tour, J. M. Nanotubes in Microwave Fields: Light Emission, Intense Heat, Outgassing, and Reconstruction. *Chem. Mater.* **2003**, *15*, 3969–3970.

(18) Kim, J.; So, H.-M.; Kim, N.; Kim, J.-J.; Kang, K. Microwave Response of Individual Multiwall Carbon Nanotubes. *Phys. Rev. B: Condens. Matter Mater. Phys.* **2004**, *70*, 153402.

(19) Paton, K. R.; Windle, A. H. Efficient Microwave Energy Absorption by Carbon Nanotubes. *Carbon* **2008**, *46*, 1935–1941.

(20) Vázquez, E.; Prato, M. Carbon Nanotubes and Microwaves: Interactions, Responses, and Applications. *ACS Nano* **2009**, *3*, 3819–3824.

(21) Ye, Z.; Deering, W. D.; Krokhin, A.; Roberts, J. A. Microwave Absorption by an Array of Carbon Nanotubes: A Phenomenological Model. *Phys. Rev. B: Condens. Matter Mater. Phys.* **2006**, *74*, 075425.

(22) Bhandavat, R.; Kuhn, W.; Mansfield, E.; Lehman, J.; Singh, G. Synthesis of Polymer-Derived Ceramic Si(B)CN-Carbon Nanotube Composite by Microwave-Induced Interfacial Polarization. *ACS Appl. Mater. Interfaces* **2012**, *4*, 11–16.

(23) Higginbotham, A. L.; Moloney, P. G.; Waid, M. C.; Duque, J. G.; Kittrell, C.; Schmidt, H. K.; Stephenson, J. J.; Arepalli, S.; Yowell, L. L.; Tour, J. M. Carbon Nanotube Composite Curing Through Absorption of Microwave Radiation. *Compos. Sci. Technol.* **2008**, *68*, 3087–3092.

(24) Rangari, V. K.; Bhuyan, M. S.; Jeelani, S. Microwave Curing of CNFs/EPON-862 Nanocomposites and Their Thermal and Mechanical Properties. *Composites, Part A* **2011**, *42*, 849–858.

(25) Du, J.; Wang, S.; You, H.; Zhao, X. Understanding the Toxicity of Carbon Nanotubes in the Environment is Crucial to the Control of Nanomaterials in Producing and Processing and the Assessment of Health Risk for Human: A Review. *Environ. Toxicol. Pharmacol.* **2013**, *36*, 451–462.

(26) Zhao, X.; Liu, R. Recent Progress and Perspectives on the Toxicity of Carbon Nanotubes at Organism, Organ, Cell, and Biomacromolecule Levels. *Environ. Int.* **2012**, *40*, 244–255.

(27) Kosynkin, D. V.; Higginbotham, A. L.; Sinitskii, A.; Lomeda, J. R.; Dimiev, A.; Price, B. K.; Tour, J. M. Longitudinal Unzipping of Carbon Nanotubes to Form Graphene Nanoribbons. *Nature* **2009**, *458*, 872–876.

(28) Rafiee, M. A.; Lu, W.; Thomas, A. V.; Zandiatashbar, A.; Rafiee, J.; Tour, J. M.; Koratkar, N. A. Graphene Nanoribbon Composites. *ACS Nano* **2010**, *4*, 7415–7420.

(29) Liu, M.; Zhang, C.; Tjiu, W. W.; Yang, Z.; Wang, W.; Liu, T. One-step Hybridization of Graphene Nanoribbons with Carbon Nanotubes and Its Strong-Yet-Ductile Thermoplastic Polyurethane Composites. *Polymer* **2013**, *54*, 3124–3130.

(30) Peng, Q.; Li, Y.; He, X.; Gui, X.; Shang, Y.; Wang, C.; Wang, C.; Zhao, W.; Du, S.; Shi, E.; Li, P.; Wu, C.; Cao, A. Graphene Nanoribbon Aerogels Unzipped from Carbon Nanotube Sponges. *Adv. Mater.* **2014**, *26*, 3241–3247.

(31) Nadiv, R.; Shtein, M.; Buzaglo, M.; Peretz-Damari, S.; Kovalchuk, A.; Wang, T.; Tour, J. M.; Regev, O. Graphene – Nanoribbon Polymer Composites: The Critical Role of Edge Functionalization. *Carbon* **2016**, *99*, 444–450.

(32) Genorio, B.; Lu, W.; Dimiev, A. M.; Zhu, Y.; Raji, A.-R. O.; Novosel, B.; Alemany, L. B.; Tour, J. M. In Situ Intercalation Replacement and Selective Functionalization of Graphene Nanoribbon Stacks. *ACS Nano* **2012**, *6*, 4231–4240.

(33) Shahsavari, R.; Ulm, F.-J. Indentation analysis of fractional viscoelastic solids. *J. Mech. Mater. Struct.* **2009**, *4*, 523–550.

DOI: 10.1021/acsami.6b01756
ACS Appl. Mater. Interfaces 2016, 8, 12985–12991